VI International Conference on Computational Methods for Coupled Problems in Science and Engineering
COUPLED PROBLEMS 2015
B. Schrefler, E. Oñate and M. Papadrakakis(Eds)

MODELLING OF AIR CHAMBER SUPPORTED FLOATING PLATFORMS – COUPLING FREE SURFACE FLOW, COMPRESSIBLE AIR, AND FLEXIBLE STRUCTURES

Florian TOTH*, Manfred KALTENBACHER† and Franz G. RAMMERSTORFER*

*Institute of Lightweight Design and Structural Biomechanics
Vienna University of Technology
Gusshausstrasse 27-29, 1040 Vienna, Austria
e-mail: ftoth@ilsb.tuwien.ac.at – Web page: http://www.ilsb.tuwien.ac.at

†Institute of Mechanics and Mechatronics
Vienna University of Technology
Getreidemarkt 9, 1060 Vienna, Austria
e-mail: manfred.kaltenbacher@tuwien.ac.at – Web page: http://www.mec.tuwien.ac.at

Key words: Finite Element Method, Surface Waves, Flexible Structure, Acoustics

Abstract. Air chamber supported floating platforms can significantly decrease wave induced structural responses. Novel applications, like floating arrays of solar collectors, with low payload requirements allow the design of floating platforms supported by large, cylindrical air chambers made of highly flexible membranes. In order to predict the dynamics of such systems a modelling strategy capturing all important phenomena: incompressible free surface flow, compressible air and flexible structures is presented. The governing partial differential equations and boundary conditions are given in their linearised form, and subsequently solved by the finite element method. A frequency domain formulation is chosen to compute the steady state response to harmonic excitation. In order to handle problems in unbounded domains a perfectly matched layer formulation is used. Thereby, radiating waves are efficiently damped at the edge of the computational domain. For the sake of simplicity we present two-dimensional, test problems used for the validation of the developed modelling strategy. Finally, we present a fully coupled simulation of wave interactions with a flexible, air chamber supported floating platform.

1 INTRODUCTION

Air chamber supported platforms typically consist of a plate-like structure which is carried by a number of air chambers. The chambers are formed by vertical walls extending from the plate-like structure into the water. The lower end of the air chambers is formed

by the free water surface. Thus, in a static situation, the equilibrium air pressure in the chamber is proportional to the weight of the platform. Travelling waves will change the volume of the chamber which leads to pressure variations and hence to a dynamic excitation of the structure.

The concept of air chamber supported floating platforms was pioneered by Pinkster and Meevers Scholte, who showed that air chambers can significantly reduce wave induced forces [14]. Early works assumed spatially constant pressure in the air chambers [13, 15], which is valid if the fundamental frequency of the first acoustic mode is well above the highest expected wave frequency. Using a semi-analytic approach for the acoustic modes in the air chamber, Lee and Newman [11] derived a model which takes spatially varying air pressure in a rigid chamber into account. The governing Laplace equation in the semi-infinite water domain is solved by the boundary element method (BEM). Small deformations of the platform structure can be taken into account by the use of generalised modal coordinates [7, 19]. The air chambers of all platform concepts investigated to date have relatively stiff bounding walls [6, 7, 14, 18, 19], allowing no significant volume change due to chamber deformations. These strong bounding walls are required because of the high payload requirements (in terms of mass) of the platforms.

For novel target applications, e.g. offshore solar collectors, these payload requirement can be as low as 25 kg/m^2. Therefore, the internal pressure in the air chamber is less than 1 MPa. This allows for air chambers being formed of cylindrical, highly flexible polymer membranes. When modelling such systems the deformation of the chamber walls due to pressure oscillations must be taken into account, because they lead to significant changes in the volume, which in turn influences the pressure: the system is strongly coupled.

2 PROBLEM FORMULATION

As an example a two-dimensional problem is depicted in Fig. 1. An arc-shaped flexible structure is partially submerged in water. It is entrapping compressible air, thereby forming an air chamber. All formulations are developed for the general three-dimensional case.

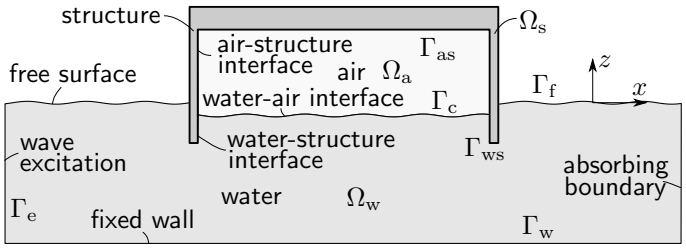

Figure 1: Sketch of the model domains.

2.1 Field Equations

Wave interaction problems require the modelling of unsteady free surface flow in the water domain denoted by Ω_w. A common modelling assumption in marine engineering is to idealise the water as an inviscid, incompressible fluid [3]. The governing equation then is the Laplace equation written as

$$-\nabla^2 p_\mathrm{w} = 0, \tag{1}$$

where ∇^2 denotes the Laplace operator, and p_w denotes the dynamic pressure in the water domain.

For the air in the chamber, i.e. the air domain Ω_a, compressibility must be taken into account. The air in the chamber is modelled as an ideal gas undergoing reversible, adiabatic changes. Furthermore, the dynamic changes in pressure, p_a, are assumed small in comparison with the static pressure and the gas is considered as inviscid. The governing equation then is the linear acoustic wave equation

$$\frac{1}{c_\mathrm{a}^2}\frac{\partial^2 p_\mathrm{a}}{\partial t^2} - \nabla^2 p_\mathrm{a} = 0\,, \tag{2}$$

where c_a is the speed of sound in the medium.

The wall of the air chamber, i.e. the structure domain Ω_s, will be considered as a linear elastic, isotropic solid. The governing equations then are the balance of momentum, the constitutive relation (Hooke's law), and the linearised strain displacement relationship

$$\rho\frac{\partial^2 \boldsymbol{u}}{\partial t^2} = \boldsymbol{\nabla}\cdot\boldsymbol{\sigma}\,, \tag{3a}$$

$$\boldsymbol{\sigma} = \boldsymbol{C}\boldsymbol{\epsilon}, \tag{3b}$$

$$\boldsymbol{\epsilon} = \frac{1}{2}\left(\boldsymbol{\nabla}\boldsymbol{u} + (\boldsymbol{\nabla}\boldsymbol{u})^T\right)\,, \tag{3c}$$

where $\boldsymbol{u}$ denotes the displacement vector, $\boldsymbol{\sigma}$ the (Cauchy-)stress tensor, $\boldsymbol{C}$ the stiffness tensor, and $\boldsymbol{\epsilon}$ the strain tensor. The juxtaposition of two elements, i.e. tensors of rank 0, 1, 2, or 4, denotes their dyadic product. Body forces were not included in the balance of momentum.

2.2 Boundary and Coupling Conditions

At the water surface both the dynamic boundary condition, i.e. the equality of the total pressure in water and air, and the kinematic boundary condition, i.e. interface particles must stay on the interface, have to be fulfilled. Introducing a coordinate system with the x-y-plane coinciding with the undisturbed water surface and the z axis pointing upwards against the vector of gravity, the hydrostatic pressure in the water domain is $p_{\mathrm{w},0} = p_{\mathrm{a},0} - \rho_\mathrm{w} g z$, where ρ_w denotes the mass density of water. The hydrostatic pressure

in the air, $p_{\mathrm{a},0}$, is assumed constant. The interface between air and water can be described by the function $z = \eta(x, y, t)$. Requiring equality of the total pressure, composed of hydrostatic and dynamic pressure, in water and air yields

$$p_{\mathrm{w}} - p_{\mathrm{a}} = \rho_{\mathrm{w}} g \eta \quad \text{on } \Gamma_{\mathrm{c}} \,. \tag{4}$$

The kinematic boundary condition, linearised and combined with the balance of momentum, yields

$$-\rho_i \frac{\partial^2 \eta}{\partial t^2} = \frac{\partial p_i}{\partial \boldsymbol{n}_\eta} \quad \text{on } \Gamma_{\mathrm{c}} \,, \tag{5}$$

where the index i is used for the water and air domain, respectively, and $\boldsymbol{n}_\eta$ denotes the normal vector of the water surface. In case of the free surface, i.e. water surface not coupled to compressible air, the dynamic boundary condition reduces to $p_{\mathrm{w}} = \rho_{\mathrm{w}} g \eta$ which can be used to eliminate η form the above equation giving

$$-\frac{1}{g} \frac{\partial^2 p_{\mathrm{w}}}{\partial t^2} = \frac{\partial p_{\mathrm{w}}}{\partial \boldsymbol{n}_\eta} \quad \text{on } \Gamma_{\mathrm{f}} \,. \tag{6}$$

At the solid-fluid interfaces between air/water and chamber wall the velocities perpendicular to the wall must be equal. In combination with the linearised momentum equation for the fluid one obtains

$$-\frac{1}{\rho_i} \nabla p_i \cdot \boldsymbol{n}_{\mathrm{s}} = \frac{\partial^2 \boldsymbol{u}}{\partial t^2} \cdot \boldsymbol{n}_{\mathrm{s}} \quad \text{on } \Gamma_{\mathrm{is}} \,, \tag{7}$$

where $\boldsymbol{n}_{\mathrm{s}}$ is the normal vector of the interface. The second coupling condition at the interface is the equality of surface stress and fluid pressure written as

$$\boldsymbol{\sigma} \cdot \boldsymbol{n}_{\mathrm{s}} = -p_i \boldsymbol{n}_{\mathrm{s}} \quad \text{on } \Gamma_{\mathrm{is}}. \tag{8}$$

The case of a stationary rigid wall can be considered as a special case of fluid structure coupling with immovable structure. The boundary condition then becomes

$$-\frac{1}{\rho_i} \nabla p_i \cdot \boldsymbol{n}_{\mathrm{s}} = 0 \quad \text{on } \Gamma_{\mathrm{w}} \,. \tag{9}$$

Waves in the fluid domain are generated by specifying a Neumann boundary condition for the pressure in the form

$$\frac{\partial p_i}{\partial \boldsymbol{n}} = f(x, y, z, t) \quad \text{on } \Gamma_{\mathrm{e}} \,, \tag{10}$$

where f is a known forcing function. For propagating surface gravity waves with low amplitude an analytical solution for the pressure field is known [9, 12], and can be used to compute the forcing function.

2.3 Perfectly Matched Layer Formulation

When studying wave propagation in semi-infinite domains the waves must be allowed to leave the finite computational domain. Therefore, a perfectly matched layer (PML) formulation is used to absorb outgoing waves without reflection. The water domain of interest, Ω_{w}, is surrounded by a PML of thickness L_k in each coordinate direction k. In this PML region, Ω_{PML}, we introduce to the complex change of variables

$$\tilde{x}_k(x_k) = x_k + \frac{1}{j\omega} \int_0^{x_k} \sigma_k(x) \, \mathrm{d}x \,; \quad x_k \in \{x, y, z\} \,, \tag{11}$$

according to Teixeira and Chew [16]. The damping function σ_k is positive inside Ω_{PML} and vanishes in Ω_{w}. Hence, we obtain the following relations

$$\frac{\partial \tilde{x}_k}{\partial x_k} = 1 + \frac{\sigma_k}{j\omega} = \zeta_k \quad \text{and} \quad \frac{\partial}{\partial \tilde{x}_k} = \frac{1}{\zeta_k} \frac{\partial}{\partial x_k} \,. \tag{12}$$

Performing a Fourier transform of the governing equation, Eq. (1), and the free surface boundary condition, Eq. (6), and inserting above relations we obtain the modified equations, which have to be solved in Ω_{PML}

$$-\frac{\partial}{\partial x}\left(\frac{1}{\zeta_x}\frac{\partial \hat{p}_{\mathrm{w}}}{\partial x}\right) - \frac{\partial}{\partial y}\left(\frac{1}{\zeta_y}\frac{\partial \hat{p}_{\mathrm{w}}}{\partial y}\right) - \frac{\partial}{\partial z}\left(\frac{1}{\zeta_z}\frac{\partial \hat{p}_{\mathrm{w}}}{\partial z}\right) = 0 \,; \qquad \frac{\partial \hat{p}_{\mathrm{w}}}{\partial \boldsymbol{n}} = \frac{w^2}{g}\hat{p}_{\mathrm{w}} \,, \tag{13}$$

with

$$\zeta_x = 1 + \frac{\sigma_x}{j\omega} \,; \quad \zeta_y = 1 + \frac{\sigma_y}{j\omega} \,; \quad \zeta_z = 1 + \frac{\sigma_z}{j\omega} \,. \tag{14}$$

The proper choice of the damping functions is of great importance, especially in order to obtain a very robust and efficient PML-technique [4]. A wave travelling through the PML region with a speed of c_p will be damped, but totally reflected at the outer boundary of the PML region. Assuming a layer thickness of L, e.g. in x-direction, the reflected wave reaches the interface between propagation and PML region with an amplitude of

$$\hat{p}_{\mathrm{w}} = p_0 e^{-(2/c_p)\cos\alpha \int_0^L \sigma_x(x)dx} = p_0 R \,. \tag{15}$$

Here, α models the angle with respect to the x-axis. In the choice of the reflection factor R the trade-off between the necessity of sufficient reduction of reflected waves according to Eq. (15) and possible disturbances of the numerical solution by a too rapid damping in a narrow PML region has to be taken into account. In our computations we use a value of $R = 10^{-3}$. Using Eq. (15) one obtains the relations:

- constant damping

$$\sigma_x^{\mathrm{const}} = \frac{-c_p \ln R}{2L\cos\varphi} \,,$$

- quadratically increasing damping

$$\sigma_x^{\text{quad}} = \frac{3c_p \ln R}{2L\cos\varphi}\,\frac{x^2}{L^2}\,,$$

- inverse distance damping

$$\sigma_x^{\text{inverse}} = \frac{c_p}{L-x}\,,$$

for different types of damping functions (for details see [8]). All of them were chosen directly proportional to the speed of the surface wave $c_p = \frac{\omega}{k} = \frac{g}{\omega}$ to remove the dependence on the wave frequency. As shown by Bermúdez et al. [2], the inverse distance damping function leads to an optimal damping behaviour for the acoustic wave equation in the frequency domain, and compared to other damping functions does not need specification of the reflection coefficient R. Within our numerical investigations, we will demonstrate that this is also true for our equation.

3 FINITE ELEMENT FORMULATION

To derive the FE formulation of the coupled problem, we assume a computational domain as displayed in Fig. 1 and just extend it by Ω_{PML} surrounding the water region Ω_{w}. Since we are interested in the time harmonic solution, we first perform a Fourier transform of the PDEs. The hat symbol, e.g. $\hat{p}$, is used to denote the Fourier transform of a quantity, e.g. p, and ω denotes the angular frequency. In order to arrive at the FE formulation, we introduce appropriate test functions φ, ψ, $\boldsymbol{\delta}$ and μ, multiply our coupled system of PDEs by these test functions and integrate over the whole computational domain. Furthermore, integration by parts* and incorporation of the boundary conditions, yields the weak (variational) formulation: Find $\hat{\boldsymbol{u}} \in (H_0^1)^3$, $\hat{p}_{\text{w}} \in H_0^1$, $\hat{p}_{\text{a}} \in H_0^1$, and $\hat{\eta} \in H_0^1$ such that†

$$\int_{\Omega_{\text{w}}} \boldsymbol{\nabla}\varphi \cdot \boldsymbol{\nabla}\hat{p}_{\text{w}}\,\mathrm{d}x - \int_{\Gamma_{\text{f}}} \frac{\omega^2}{g}\varphi\hat{p}_{\text{w}}\,\mathrm{d}s - \int_{\Gamma_{\text{c}}} \rho_{\text{w}}\omega^2\varphi\hat{\eta}\,\mathrm{d}s - \int_{\Gamma_{\text{ws}}} \rho_{\text{w}}\omega^2\varphi\hat{\boldsymbol{u}}\cdot\boldsymbol{n}_{\text{s}}\,\mathrm{d}s = \int_{\Gamma_{\text{w}}} \varphi\hat{f}\,\mathrm{d}s\,, \quad (16a)$$

$$\int_{\Omega_{\text{PML}}} \tilde{\boldsymbol{\nabla}}\varphi \cdot \tilde{\boldsymbol{\nabla}}\hat{p}_{\text{w}}\,\mathrm{d}x - \int_{\Gamma_{\text{f}}} \frac{\omega^2}{g}\varphi\hat{p}_{\text{w}}\,\mathrm{d}s = 0\,, \quad (16b)$$

*Using the relation $\boldsymbol{\nabla}\cdot(\boldsymbol{\delta}\cdot\boldsymbol{\sigma}) = (\boldsymbol{\nabla}\cdot\boldsymbol{\sigma})\cdot\boldsymbol{\delta} + \boldsymbol{\sigma} : (\boldsymbol{\nabla}\boldsymbol{\delta})$, where ':' denotes the double dot product, i.e. the sum of the products of conjugated tensor elements.

†H_0^1 is the space of functions, which are square integrable along with their first derivatives in a weak sense [1].

$$-\int_{\Omega_\mathrm{a}} \frac{\omega^2}{c_\mathrm{a}^2}\psi\hat{p}_\mathrm{a}\,\mathrm{d}x + \int_{\Omega_\mathrm{a}} \boldsymbol{\nabla}\psi\cdot\boldsymbol{\nabla}\hat{p}_\mathrm{a}\,\mathrm{d}x + \int_{\Gamma_\mathrm{c}} \rho_\mathrm{a}\omega^2\psi\hat{\eta}\,\mathrm{d}s - \int_{\Gamma_\mathrm{as}} \rho_\mathrm{a}\omega^2\psi\hat{\boldsymbol{u}}\cdot\boldsymbol{n}_\mathrm{s}\,\mathrm{d}s = 0\,, \tag{16c}$$

$$-\int_{\Omega_\mathrm{s}} \rho_\mathrm{s}\omega^2\boldsymbol{\delta}\cdot\hat{\boldsymbol{u}}\,\mathrm{d}x + \frac{1}{2}\int_{\Omega_\mathrm{s}} \boldsymbol{\nabla}\boldsymbol{\delta} : \boldsymbol{C}\left(\boldsymbol{\nabla}\hat{\boldsymbol{u}} + (\boldsymbol{\nabla}\hat{\boldsymbol{u}})^T\right)\mathrm{d}x$$
$$-\int_{\Gamma_\mathrm{ws}} \hat{p}_\mathrm{w}\boldsymbol{n}_\mathrm{s}\cdot\boldsymbol{\delta}\,\mathrm{d}s - \int_{\Gamma_\mathrm{as}} \hat{p}_\mathrm{a}\boldsymbol{n}_\mathrm{s}\cdot\boldsymbol{\delta}\,\mathrm{d}s = 0\,, \tag{16d}$$

$$\int_{\Gamma_\mathrm{c}} \mu\hat{p}_\mathrm{w}\,\mathrm{d}s - \int_{\Gamma_\mathrm{c}} \mu\hat{p}_\mathrm{a}\,\mathrm{d}s - \int_{\Gamma_\mathrm{c}} \mu\rho_\mathrm{w}g\hat{\eta}\,\mathrm{d}s = 0\,, \tag{16e}$$

for all test functions $\varphi \in H_0^1$, $\psi \in H_0^1$, $\boldsymbol{\delta} \in (H_0^1)^3$, and $\mu \in H_0^1$. It has to be noted that the surface elevation η acts as a Lagrange-multiplier to enforce the interface condition between water and air along Γ_c. The scaled Nabla-operator $\tilde{\boldsymbol{\nabla}}$ in Eq. (16b) computes according to Eqs. (13) and (14)

$$\tilde{\boldsymbol{\nabla}} = \left(\frac{1}{\zeta_x}\frac{\partial}{\partial x}\,,\ \frac{1}{\zeta_y}\frac{\partial}{\partial y}\,,\ \frac{1}{\zeta_z}\frac{\partial}{\partial z}\right)^T\,. \tag{17}$$

Furthermore, we want to note that the complex change of variables according to Eq. (11) has also to be performed, when computing the Jacobian within the FE procedure for Eq. (16b).

For the spatial discretisation we apply standard quadrilateral finite elements of 2nd order. The whole scheme has been implemented in the in-house research software CFS++ (Coupled Field Simulation) and used to compute the results presented in the following section. For some comparison, we have also applied the commercial software Abaqus [5].

4 RESULTS OF TEST PROBLEMS

Various numerical tests were carried out in order to validate the implementation of the described equations. The assumed material properties are given in Table 1(a). For the acceleration of gravity, g, a value of 9.81 m/s^2 was assumed. For the sake of simplicity two-dimensional problems are presented in the following.

Table 1: Assumed material properties for the fluids (a), and linear elastic, isotropic solid (b).

(a) Fluid properties

Property	Air	Water
c_i in m/s	343.05	1484.58
ρ_i in kg/m^3	1.2041	998.2

(b) Solid properties

E in MPa	800.0
ν	0.3
ρ in kg/m^3	1000.0

Table 2: Sloshing frequencies for the anticipated geometry.

Mode number n	0	1	2	3	4	5	6
Frequency in Hz	0.0306	0.0565	0.0764	0.0910	0.1044	0.1152	0.1247

4.1 Sloshing

In order to test the free surface boundary condition alone, the natural modes of a two-dimensional, rectangular tank with length $l = 350$ m and a water depth of $h = 50$ m were computed numerically. The domain was discretised by finite elements and the appropriate boundary conditions were applied (stationary wall at the left, bottom and right side; free surface condition at the top). The natural frequencies and corresponding mode shapes were computed by solving the standard eigenvalue problem which is obtained from the discretised ordinary differential equation system by making an harmonic Ansatz for the time dependant pressure. The obtained natural frequencies are given in Table 2. Comparison with the known analytical solution [9, 10] showed excellent agreement.

4.2 Travelling Waves

In order to test the efficiency of the PML formulation in a further test example a rectangular domain of water of uniform depth h=50 m was considered. The length of the domain was 350 m. Steady state solution of travelling waves were computed in a harmonic analyses at a range of wave frequencies. Waves were generated on the left wall, and a PML was used to absorb them at the right boundary.

If the absorption is not perfect, a part of the wave is reflected, and a superposition of waves travelling in positive and negative direction is obtained. The combined wave system shows a spatially varying amplitude. The reflection coefficient, i.e. the ratio between the amplitude of the reflected wave and the amplitude of the incident wave, can be computed by

$$\frac{a_{\text{ref}}}{a_{\text{inc}}} = \frac{a_{\max} - a_{\min}}{a_{\max} + a_{\min}}, \tag{18}$$

where $a_{\max}$ is the maximum amplitude of the combined wave system, and $a_{\min}$ is the minimum amplitude of the combined wave system.

The impact of the thickness of the PML was investigated by comparing results from computations with PMLs consisting of 1, 2, 4 and 8 finite elements, respectively. For all computations elements with 2nd order basis functions were used. The functions for the quadratically increasing as well as inverse distance damping were accordingly adjusted in each integration point. The results obtained for a wave frequency of 0.1 Hz, displayed in Fig. 2(a), demonstrate the extreme performance of the inverse distance damping function, which already shows an optimal performance with a layer thickness of just one finite element.

In Fig. 2(b) a comparison of the PML formulation with inverse damping function and acoustic infinite elements implemented in Abaqus [5] is shown for a range of wave

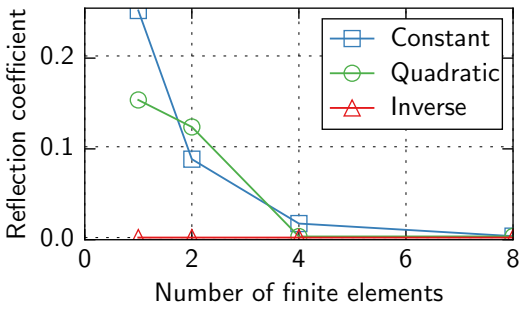

(a) Comparison of different damping functions at a wave frequency of 0.1 Hz.

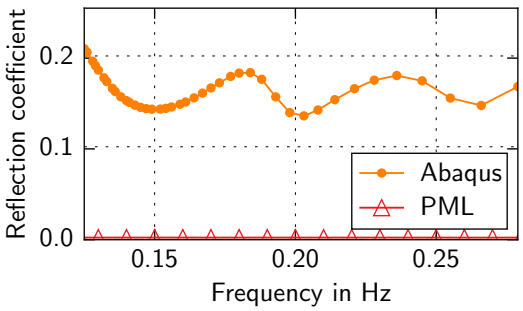

(b) Comparison of Abaqus infinite elements and PML with inverse damping function.

Figure 2: Reflection coefficient in dependence of PML thickness (a) and wave frequency (b).

frequencies. The acoustic infinite elements in Abaqus are designed for the absorption of sound waves. In order to achieve absorption of surface gravity waves, the compressibility of the acoustic medium of the acoustic infinite elements was modified such that the speed of sound equals the wave speed of surface gravity waves. Therefore, the compressibility was set to $K_{\text{inf}} = \rho_{\text{w}} \left(\frac{g}{\omega}\right)^2$. The PML formulation with inverse damping function shows the best performance (with almost vanishing reflection coefficients) over all frequencies, due to the scaling of the damping function with speed c_p of the surface wave.

5 FLOATING STRUCTURE WITH SINGLE AIR CHAMBER

As an example of a fully coupled, two-dimensional problem a single floating air chamber as sketched in Fig. 1 was considered. A single chamber will likely become statically unstable, therefore, in a more realistic system at least three chambers must be used to provide sufficient safety against overturning [17]. The single chamber system is nevertheless chosen, because it is the simplest system to illustrate wave interaction effects with a flexible air chamber. Figure 3 shows the computed pressure in the water and the air domain. The flexible structure reflects a part of the incoming waves, visible in the spatially varying

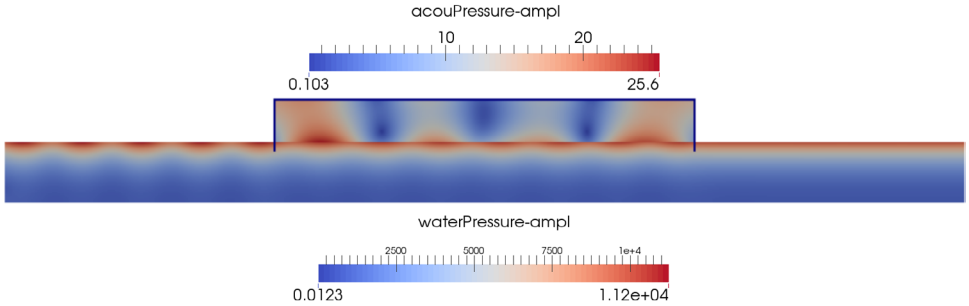

Figure 3: Computed pressure in the water and in the entrapped air. Values in Pa.

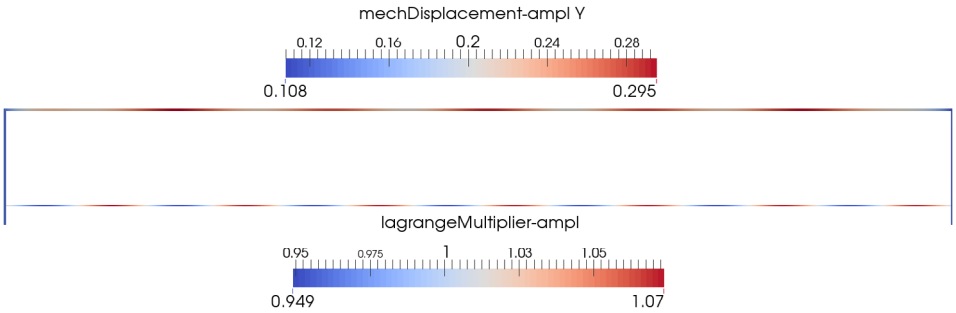

Figure 4: Computed mechanical displacement of the structure (in y-direction) and surface elevation. Values in m.

pressure amplitudes at the water surface on the left side. On the right side of the water domain, the pressure amplitude is constant, corresponding to waves propagating towards the right edge where they are completely absorbed by the PML. The wave amplitude is reduced to about 88% of the excitation amplitude behind the structure.

The structural displacements are displayed in Fig. 4, together with the surface elevation of the air-water interface, i.e. the Lagrange multiplier in the coupling equation. A combination of rigid body heave displacement, superimposed by a bending type deformation arises. The maximum displacement amplitudes are about one third of the wave amplitude.

6 CONCLUSIONS

A monolithic finite element formulation for the fully coupled analysis of incompressible free surface flow, deformable structures and compressible fluids was developed. As the formulation is based on linearised theory it is applicable to cases with sufficiently small disturbances from the equilibrium position. An harmonic formulation was chosen as it is most suitable for the analysis of wave interaction problems. To allow for the analysis of wave propagation in semi-infinite domains a highly efficient PML formulation was developed. Selected test cases were presented, to demonstrate the validity and performance of the modelling strategy.

Wave interactions with an air chamber supported floating platform were treated in a fully coupled manner. Here, the effect of a deformable chamber filled by a compressible fluid could be directly included. Typical target applications for the modelling approach are, hence, very large floating platforms, wave energy converters, or air chamber supported floating platforms. Furthermore, the presented modelling strategy can be applied to investigate sloshing effects in liquid filled tanks.

References

[1] Adams, R.A. *Sobolev Spaces*. Pure and Applied Mathematics. Academic Press, (1975).

[2] Bermúdez, A., Hervella-Nieto, L., Prieto, A., and Rodríguez, R. An optimal perfectly matched layer with unbounded absorbing function for time-harmonic acoustic scattering problems. *Journal of Computational Physics* (2007) **223**(2):469–488.

[3] Chakrabarti, S.K. *Numerical Models in Fluid-structure Interaction*. Advances in fluid mechanics. WIT, (2005).

[4] Collino, F. and Monk, P.B. Optimizing the perfectly matched layer. *Computer Methods in Applied Mechanics and Engineering* (1998) **164**:157–171.

[5] Dassault Systmes, . *Abaqus Analysis User's Manual*, 6.13-4 edition, (2013).

[6] Guret, R.A.M. *Interaction of free surface waves with elastic and air-cushion platforms*. PhD thesis, Delft University of Technology, (2003).

[7] Ikoma, T., Rheem, C.K., Maeda, H., and Masuda, K. Hydroelastic Behaviors of VLFS Supported by Many Aircushions With the Three-Dimensional Linear Theory. *Journal of Offshore Mechanics and Arctic Engineering* October (2011) **134**(1): 011104(8).

[8] Kaltenbacher, M. *Numerical Simulation of Mechatronic Sensors and Actuators*. Springer, Berlin, 2. edition, (2007). ISBN: 978-3-540-71359-3.

[9] Kundu, P.K., Cohen, I.M., and Dowling, D.R. *Fluid Mechanics*. Academic Press. Academic Press, (2012).

[10] Lamb, H. *Hydrodynamics*. Cambridge University Press, (1895).

[11] Lee, C.H. and Newman, J.N. Wave effects on large floating structures with air cushions. *Marine Structures* (2000) **13**(4-5):315–330.

[12] Lighthill, J. *Waves in Fluids (Cambridge Mathematical Library)*. Cambridge University Press, (2001).

[13] Malenica, S. and Zalar, M. An alternative method for linear hydrodynamics of air cushion supported floating bodies. In *Proceedings of the 15th IWWWFB*, (2000).

[14] Pinkster, J.A. and Meevers Scholte, E.J.A. The behaviour of a large air-supported MOB at sea. *Marine Structures* (2001) **14**(1-2):163–179.

[15] Pinkster, J. The effect of air cushions under floating offshore structures. In Vugts, J., editor, *Proceedings of the International Conference on Behaviour of Offshore Structures '97*. Pergamon, (1997).

[16] Teixeira, F. and Chew, W. Complex space approach to perfectly matched layers: a review and some developments. *International Journal of Numerical Modelling: Electronic Networks, Devices and Fields* (2000) **13**:441–455.

[17] Toth, F. *Static and Dynamic Modelling of Lightweight Floating Platforms Supported by Flexible Air Chambers*. PhD thesis, Vienna University of Technology, (2014).

[18] Tsubogo, T. and Okada, H. Hydroelastic Behavior of an Aircushion-Type Floating Structure. In Chung, J.S., Sayed, M., Kashiwagi, M., Setoguchi, T., and Hong, S.W., editors, *The Proceedings of The Twelfth (2002) International Offshore and Polar Engineering Conference*, (2002).

[19] van Kessel, J.L.F. *Aircushion Supported Mega-Floaters*. PhD thesis, Delft University of Technology, (2010).